ATLANTIS PRESS

Advances in Engineering Research, volume 114

International Conference on Advances in Materials, Machinery, Electrical Engineering (AMMEE 2017)

Numerical Simulation of Damping Capacity between Injector-Formed Baffle and Normal Blade Baffle in a Kero/LOX Liquid Rocket Engine

Kangkang Guo[a], Wansheng Nie[b], Yu Liu[c], Honghua Cai[d]

Department of Space Equipment, Equipment Academy, Beijing 101416, China

[a]guokangkang@sjtu.enu.cn, [b]nws1969@126.com, [c]liuyu@nudt.edu.cn, [d]honghuacai@aliyun.com

Keywords: Kero/LOX liquid rocket engine, high frequency combustion instability, heat release, thermo-acoustic coupling, injector-formed baffle, normal blade baffle.

Abstract. The topic of this paper is the damping capacity of injector-formed baffle and normal blade baffle in a liquid rocket propellant rocket engine. High frequency combustion instability of a liquid rocket engine is investigated numerically, and the mechanism of high frequency unstable combustion is analyzed. Results shows that the pressure oscillates in phase with the heat release, which is accord with the Rayleigh criterion. Injector-formed baffle and two kinds of normal blade baffle are designed and calculated when all three kinds of length of baffle is 30mm. Numerical results demonstrate that injector-formed baffle can suppress the 1T mode instability completely while other two kinds of normal blade baffle can't. A conclusion can be reached that injector-formed baffle has higher damping capacity, which results from the viscous or frictional force from gaps between two adjoining injectors. Further speaking, viscous force generating from gaps can dissipates the oscillation energy quickly.

1. Introduction

High frequency combustion instability is still a challenging problem in the development of liquid rocket engine. Advanced Large thrust rocket engine is a prominent demand of the farther space exploration, however, high frequency unstable combustion acts as a big obstacle in the way. High frequency instability, also known as acoustic instability, is characterized by undesirable pressure fluctuations whose peak-to-peak amplitude exceeds 10% of average chamber pressure and whose pressure vibration frequency corresponds with eigen acoustic modes of the chamber [1]. High frequency combustion instability is extraordinarily destructive, especially the 1T (The first-order tangential) mode, which can destroy the cooling fluid film attached to the chamber wall and further lead to extensive heat transfer to the injector faceplate and chamber wall. Therefore, once the 1T mode high frequency combustion instability occurs, the combustion chamber would suffer a severe thermal ablation even the completely destroy to a great extent [2, 3].

There are two methods, active and passive controls, to suppress the high frequency unstable combustion [4]. In active method, it is believed that preventing the positive feedback between combustion and the complex of injection, vaporization, atomization, mixing and chemical reaction is the vital solution to control the high frequency combustion instability. However, it is a formidable task to realize the goal of active control, additionally, the catastrophe result from acoustic instability would appear in an extremely short time and the active control is useless because it can't response promptly [3]. On the other hand, passive control is a reliable choice. The most commonly used passive damping devices contain resonators, acoustic liners and baffles, which suppress unstable combustion by changing the acoustic characteristic of chamber and decoupling the combustion and acoustic characteristic [4].

In this paper, the high frequency unstable combustion of a Kero/LOX liquid rocket engine is investigated numerically, and the mechanism of combustion instability is analyzed. After that, the damping capability of injector-formed baffles and two kinds of normal blade baffles is studied and compared.

2. Numerical simulation model

2.1 Governing equations

Gas-center swirl-coaxial injector is applied in the targeted engine, gas O_2 is injected into chamber along the axial while the liquid kerosene swirls along the recess wall of injector before entering the chamber. As for gas phase, conservative three-dimensional N-S equation in rectangular coordinate system is used as the control equation, and the general form of the governing equation is given as follows [5].

$$\frac{\partial \vec{U}}{\partial t}+\frac{\partial(\vec{F}-\vec{F}_{\mathrm{v}})}{\partial x}+\frac{\partial(\vec{G}-\vec{G}_{\mathrm{v}})}{\partial y}+\frac{\partial(\vec{H}-\vec{H}_{\mathrm{v}})}{\partial z}=\vec{J} \tag{1}$$

Where, $\vec{U}$ is the conservative variable vector, t is the time variable, $\vec{F}$, $\vec{G}$, $\vec{H}$ and $\vec{F}_{\mathrm{v}}$, $\vec{G}_{\mathrm{v}}$, $\vec{H}_{\mathrm{v}}$ are the convection item vectors and viscous term vectors, respectively, $\vec{J}$ is the source term vector. Quality momentum equation, energy equation and equation of components in the directions of x, y and z are all included by the above equation.

When it comes to liquid phase, Lagrange particle orbital model is used. The mass, momentum and energy exchange between gas and liquid phases are realized by controlling the source term of the equation; the atomization process of the liquid phase is described by the given atomization cone and droplet diameter distribution; in this paper, atomization cone is determined as 30° and Rosin-Rammler distribution model is chosen in which average droplet diameter is 50 μm; the evaporation process is controlled by convective diffusion process [6].

2.2 Discretization scheme and solution of the equation

Finite volume method (FVM) is used to discretize the control equation mentioned above. For the strong nonlinear coupling of N-S equations, the decoupling between pressure and velocity is realized by using PISO [5, 7] (Pressure Implicit with Splitting Operator). In the process of discretizing convective terms and viscous terms, central difference scheme and Van Leer [7] scheme with second order precision is adopted in interface interpolation, respectively. As for the time term, backward difference scheme, with second order precision, is applied.

2.3 Chemical reaction mechanism

It is hard to obtain the actual chemical reaction process accurately, since kerosene is a mixture of hundreds of components. An effective method is to simplify the chemical reaction. In this paper, alternative fuel $C_{12}H_{23}$ serves as the kerosene and a single step global chemical reaction mechanism is used to describe the chemical reaction process. K_f is labeled as chemical reaction rate and calculated by formula (2) [6].

$$K_f = \mathrm{A}e^{-\mathrm{E_a}/T}c_{KERO}^{n_{KERO}}c_{O_2}^{n_{O_2}} \tag{2}$$

Where, T is the temperature with unit K; c_{KERO} and c_{O_2} is the molar concentration of kerosene and oxygen with unit mol/cm3. The specific value of the remaining parameters is shown in Table 1.

Table 1 Chemical reaction mechanism

Reaction	A	E_a	n_{KERO}	n_{O2}
$C_{12}H_{23}+17.75O_2 \rightarrow 12CO_2+11.5H_2O$	2.587E9	1.256E8	0.25	1.5

2.4 Turbulent model and turbulent combustion model

In consideration of calculated quantity, compressible RANS (Reynolds-Averaged Navier-Stokes) is adopted as the turbulent model and reliable k-ε double equation model is chosen.

The ED (eddy dissipation) model, which is established on the basis of the EBU (Eddy Break-Up) model, serves as the combustion model. In ED model, not only the effect that component transport and turbulence pulsation exert on chemical reaction rate is taken into consideration, but also chemical reaction rate is also related to the minimum concentration of oxidants, fuels and reaction products [8, 9, 10].

2.5 Grid and boundary conditions

Unstructured grid is used in paper, and the grid with injector-formed baffle is shown in Fig.1, the grid around gaps is refined as showing in enlarge window.

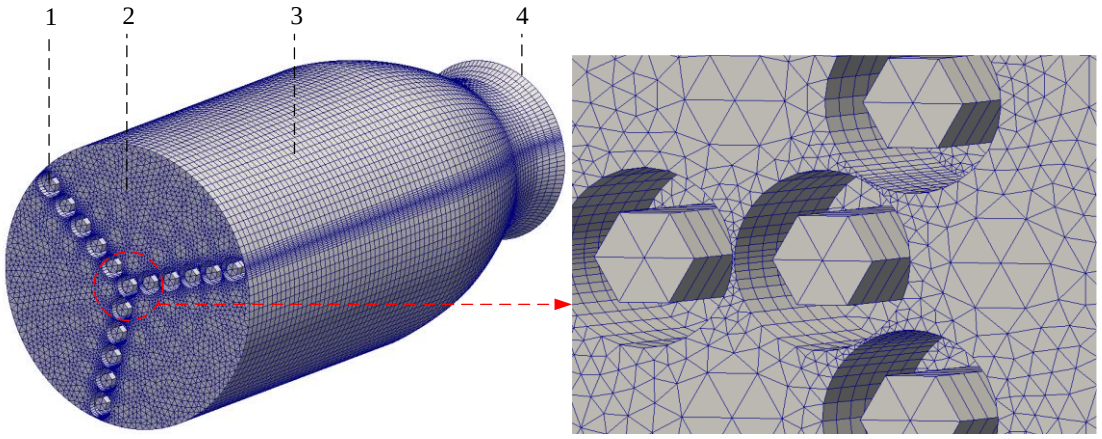

Fig.1 Grid of injector-formed baffle

Boundary conditions of the internal flow field is shown as Table 2. The configuration of the targeted liquid rocket engine and parameters is shown in Table 3.

Table 2 Boundary conditions of internal flow field

NO	name	Boundary condition
1	injector intlet	mass flow inlet
2	injector faceplate	no-slip and thermal- isolation wall
3	chamber wall	no-slip and thermal- isolation wall
4	nozzle outlet	pressure outlet

Table 3 Configuration of chamber and initial parameters

Parameters of targetted engine	Kero/LOX
diameter of chamber (mm)	180
diameter of throat (mm)	99
length of chamber (mm)	380
mass flow of fuel (kg/s)	9.1
inlet temperature of fuel (K)	450
mass flow of oxidant (kg/s)	55
inlet temperature of oxidant (K)	600
pressure of outlet (pa)	101325
temperature of outlet (K)	300k

3. Validation of numerical model

The design chamber pressure of the targeted liquid rocket engine is 12MPa when the fuel mass flow is 13.5kg/s and the O/F rate is 2.5, which is verified by experiment.

In order to validate numerical simulation model build in this paper, calculation based on the design condition is carried out. The pressure changing process is shown in Fig.2. As can be seen, the pressure of the chamber is 11.80 MPa at steady stage. The error is 1.67% compared with the experiment value, which is tolerated. Therefore, the validation of numerical simulation model can be verified.

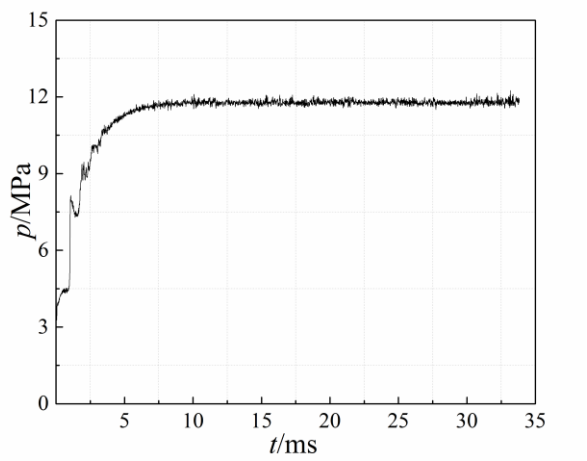

Fig.2 Pressure changing process in design condition

4. Results and analysis of numerical simulation

4.1 Analysis and mechanism high frequency combustion instability

When the inlet mass flow of fuel is 9.1kg/s and the O/F rate is 6.04, with all injectors sharing the propellant equally, there is a significant 1T instability mode coming into being. The pressure changing process is shown in Fig.3. As Fig.3 shows, the peak-to-peak amplitude of the pressure oscillations reaches 80atms, the severity of this high frequency instability is noteworthy.

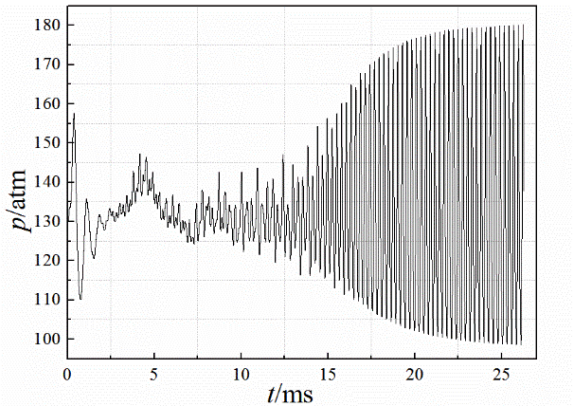

Fig.3 Pressure of 1T mode unstable combustion

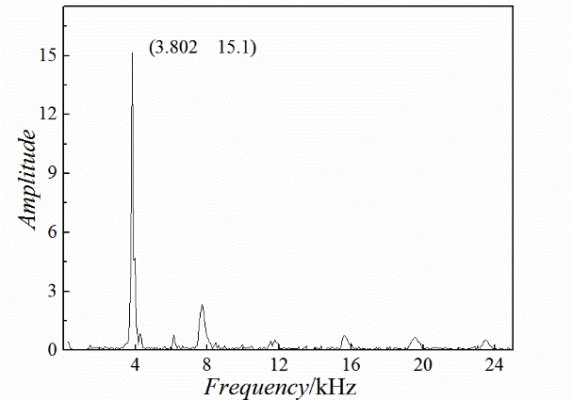

Fig.4 Frequency spectrum analysis of the instability

The corresponding frequency spectrum analysis is displayed in Fig.4 by means of FFT (Fast Fourier Transform Algorithm). As can be seen, the predominant frequency value is 3802Hz. The eigenfrequency of a chamber is determined by the geometrical configuration of chamber as well as the equilibrium acoustic velocity in working condition, which can be calculated by formula (3) [3].

$$f_{lmn} = \frac{c}{2\pi}\sqrt{\left(\frac{\lambda_{mn}^2}{R_c^2} + \frac{l^2\pi^2}{L_c^2}\right)} \qquad l, m, n = 0, 1, 2\cdots \tag{3}$$

Where, c is the acoustic velocity with unit m/s; λ_{mn} represents transverse eigenvalues; R_c is the radius of chamber with unit m, and L_c demonstrates equivalent length of chamber with unit m.

The equilibrium acoustic velocity is 1091.7m/s, which is calculated with CEA (Chemical Equilibrium with Applications) from NASA. According to formula (3), the frequency of 1Tmode is 3555Hz, which is close to the dominant frequency.

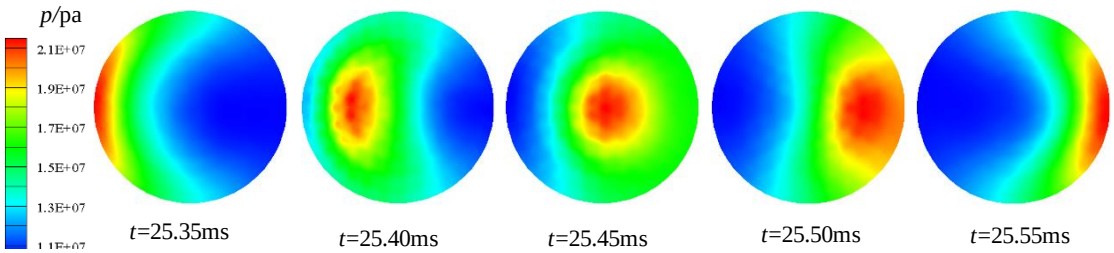

Fig.5 Pressure contours of cross section within one cycle

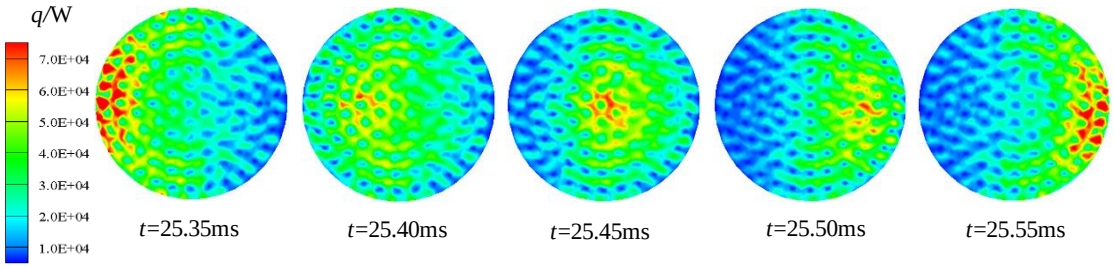

Fig.6 Heat release contours of cross section within one cycle

The errors of numerical simulation results, compared with theoretical value, is 6.95%. And the difference between theoretical value and numerical value principally results from the inequality between equilibrium acoustic velocity and local acoustic velocity.

The sustained instability is driven by the coupling between acoustic characteristic of chamber and combustion process, in a high frequency unstable combustion process, oscillations of pressure and heat release tends to be in-phase according to the reference [11,12]. In this paper, the phenomenon of homophase between pressure oscillations and heat release can be captured, which is shown in Fig.5 and Fig.6.

In the process of high frequency unstable combustion, pressure and temperature fluctuates in-phase with the fluctuations of heat release, which can be displayed in Fig.7 and Fig.8.

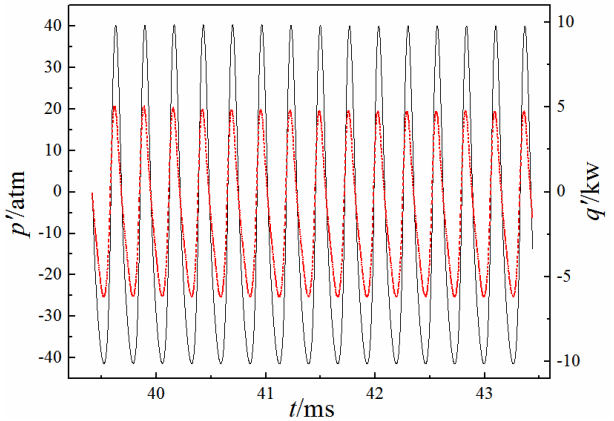

Fig.7 Changing process of pressure and heat release

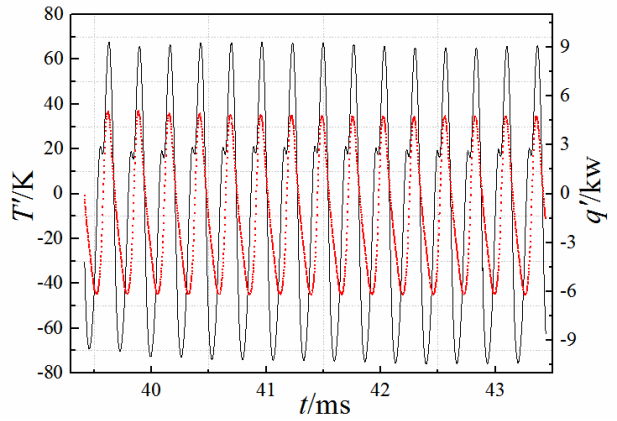

Fig.8 Changing process of temperature and heat release

Rayleigh criterion indicates that releasing heat in-phase with pressure oscillations can sustain the unstable combustion, in other words, the unstable combustion can be driven by releasing heat when the pressure arrives at maximum and absorbing heat when the pressure comes to minimum. The unstable combustion in this paper can be explained in this way, meanwhile, inhomogeneous heat release leads to temperature fluctuates in-phase.

4.2 Damping capacity of injector-formed baffle and normal blade baffle

Injector-formed baffle and two kinds of normal blade baffle, which are labeled baffle scheme1~3 and show in Fig.9, are designed and applied to suppress the 1T mode unstable combustion. It is believed that baffle with only three blades can suppress 1T mode high frequency instability effectively [14].

According to reference [14-17], the optimal damping capacity of baffled injectors can be obtained when the gaps between two adjacent injectors stay around 0.2mm, and in this paper, the value of gaps is 0.2mm. As showing in (b), this kind of normal blade baffle lengthens the injectors located along the three blades and changes the original distribution of propellant, while in (c), three blades merely extend from the injector faceplate without changing the injection position, however, the center is not closed because of the space restriction of the center injector. All the three baffle schemes are of 30mm length.

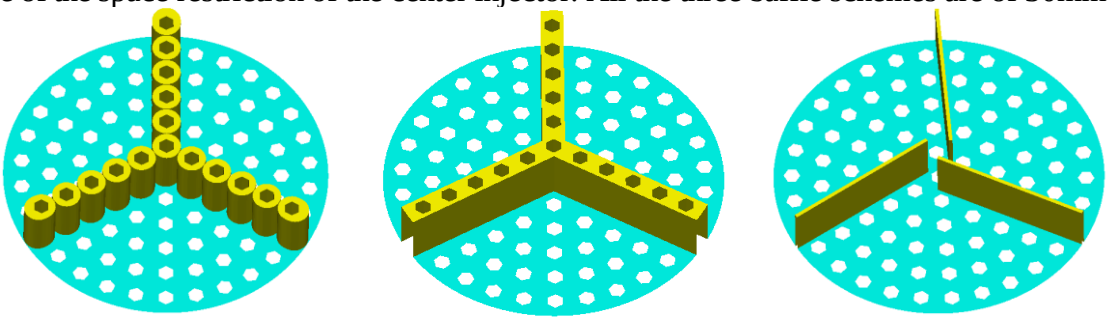

(a) Baffle scheme1 (b) Baffle scheme2 (c) Baffle scheme3

Fig.9 Injector-formed baffle and two kinds of normal blade baffle

The reason why baffle can suppress the high frequency instability is that it changes the acoustic characteristic of the chamber and further decouples the thermo-acoustic combustion instability. In the numerical simulation, monitoring point is set close to the chamber wall and 50mm downstream from the injector faceplate. Suppression effect of three baffle schemes is shown in Fig.10. It is clear that injector-formed baffle could suppress the pressure oscillations completely while the two other baffle schemes could not.

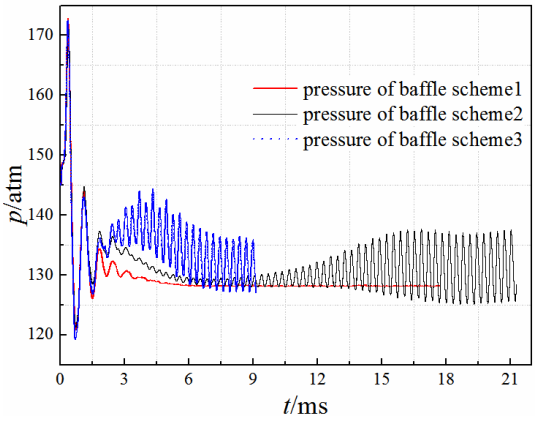

Fig.10 Suppressing effect of injector-formed baffle and two kinds of normal blade baffle

The high frequency combustion instability of baffle scheme2~3 is analyzed as Fig.11 and Fig.12, respectively, the peak-to-peak amplitude of baffle scheme2~3 are about 12atms and 14atms, separately. So the unstable combustion under scheme2~3 can't be neglected; the predominant frequency of two unsteady combustion cases are 2966Hz and 2995Hz, respectively. The interference of baffle makes the coupling frequency diverge from the frequency of unbaffled chamber. The damping capacity of sheme2~3 is insufficient to suppress the high frequency instability, letting the pressure and heat release oscillate in-phase at a lower frequency.

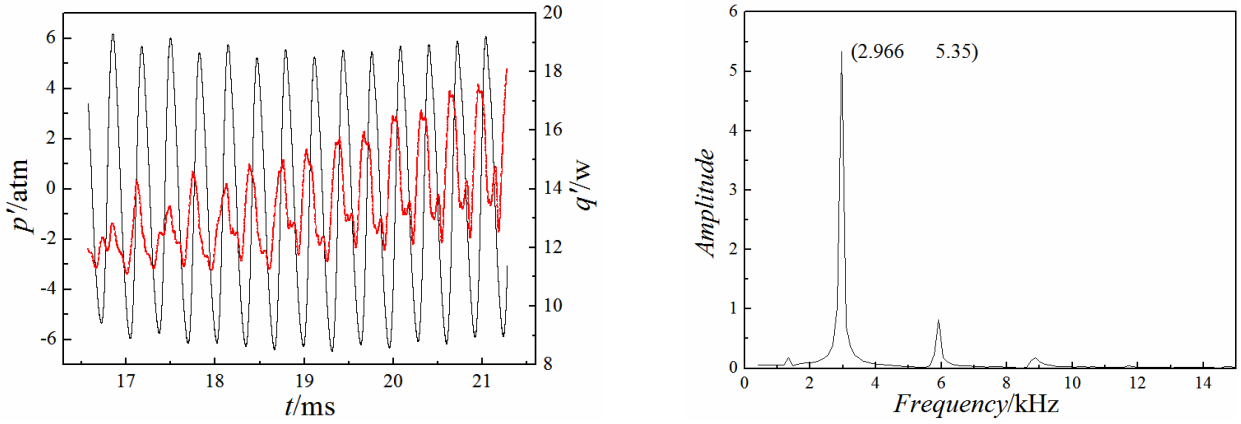

Fig.11 High frequency unstable combustion analysis of baffle scheme2

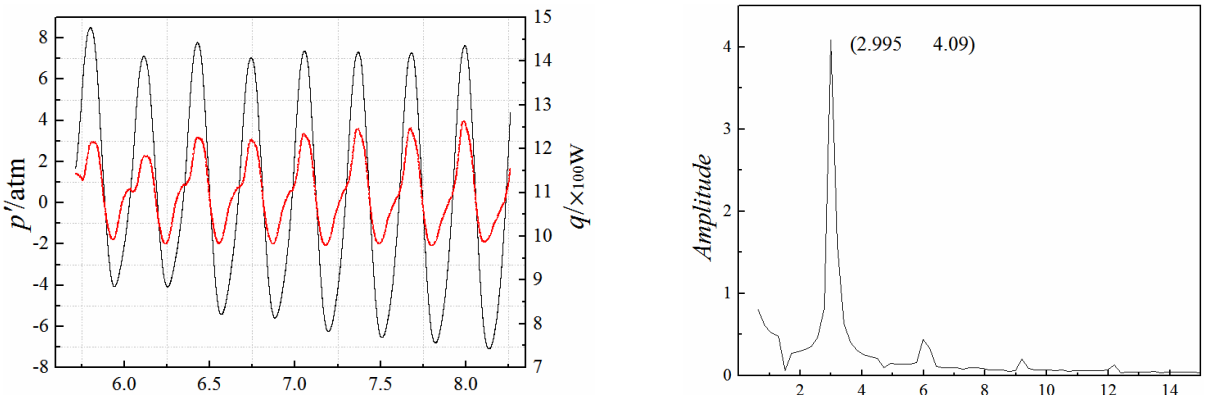

Fig.12 High frequency unstable combustion analysis of baffle scheme2

There is not adequate evidence to verify that the damping capacity of injector-formed baffle is larger than normal blade baffle because baffle scheme2 lengthens the injectors located along the three blades and the center of baffle scheme3 isn't closed. Strictly speaking, both of them are not normal blade baffle. Therefore, baffle scheme4, shown in Fig.13, is designed to offer a supplementary proof. Pressure results with the monitoring point located 50mm away from injector faceplate is shown in Fig.14. Although the center of baffle scheme4 isn't closed, the unsteady combustion is suppressed

totally, compared with the result of baffle scheme3, the conclusion that the damping capability of injector-formed baffle is higher and more effective can be reached.

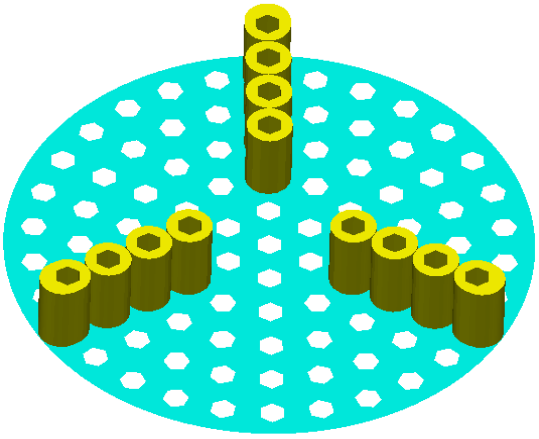

Fig.13 Configuration of baffle scheme4

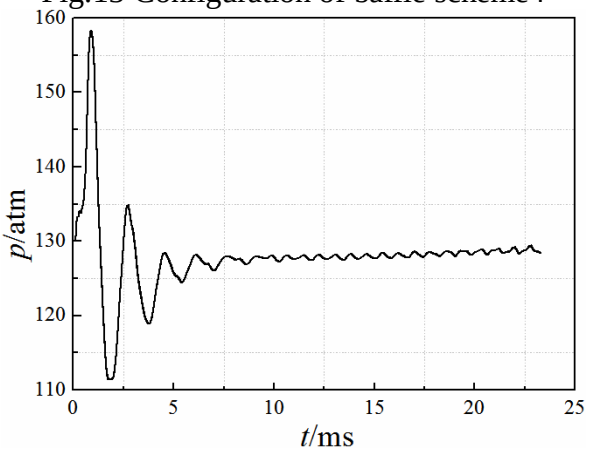

Fig.14 Pressure of baffle scheme4

4.3 Analysis of extra damping capacity of injector-formed baffle

Extra damping capacity of injector-formed baffle is considered originating from viscous dissipation between two adjacent injectors in reference [16]. It is the extra viscous force generating from adjoining gaps that makes the enhanced damping capacity of injector-formed baffle. In reference [16], the dissipation rate of kinetic energy of fluid, ε , severs as the criteria to evaluate the damping capacity.

In this paper, contours of tangential velocity and ε are shown in Fig.15 and Fig.16,respectively. Apparently, the tangential velocity in the both sides of baffled injectors blade sharply reduced to zero in the opposite direction, it looks like two flows, whose direction is opposite, bump against the baffled injectors until the speed decreases to zero, and the viscous dissipation of gaps plays a significant role in this process. what's more, the value of ε in gaps is larger than other area, which can account for the reason that extra damping capacity of injector-formed baffle. It is the high capability of energy dissipation that makes the extra damping capacity of injector-formed baffle.

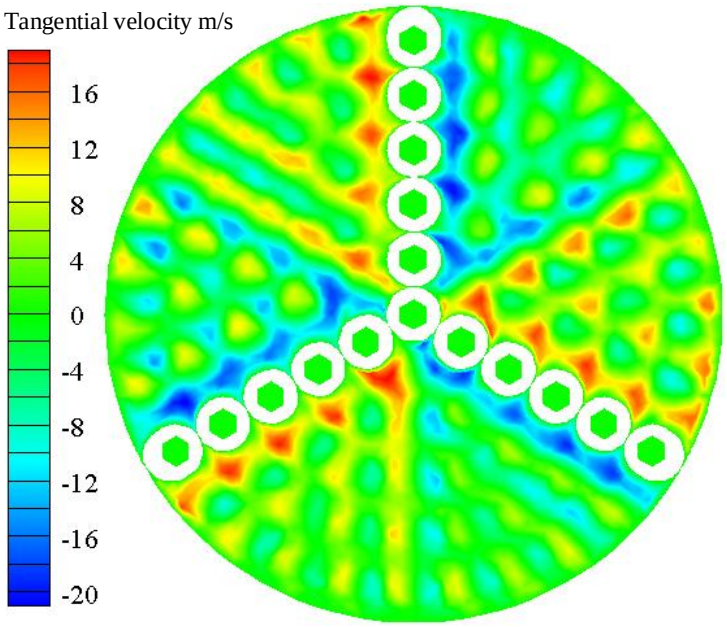

Fig.15 Tangential velocity of cross section in injector-formed baffle

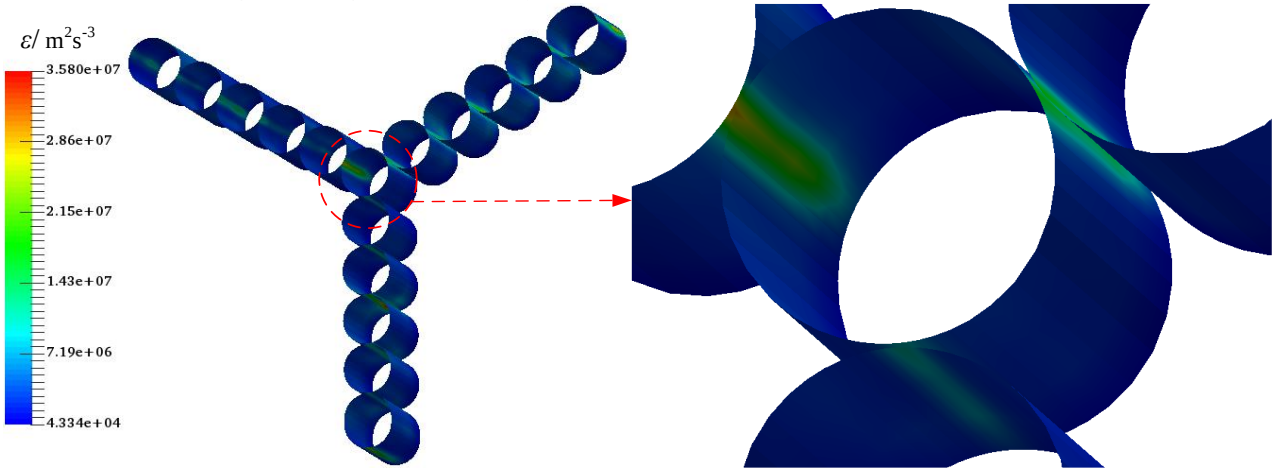

Fig.16 Contour of kinetic energy dissipation rate

5. Conclusion

(1) Once high frequency combustion instability appears, pressure oscillations is accompanied by heat release fluctuations in-phase. Meanwhile, temperature oscillates with heat release in phase. Releasing heat in-phase with pressure oscillations can sustain the unstable combustion.

(2) Injector-formed baffle can suppress the high frequency unstable combustion completely while normal blade baffle can't as the length of baffle is 30mm. Compared with unbaffled chamber, high frequency instability turns up at a lower frequency when normal blade baffle is mounted.

(3) The damping capacity of injector-formed baffle is higher than other two kinds of normal blade baffle with the same baffle length. Extra damping capacity of baffled injectors results from the viscous dissipation from gaps between two adjoining injectors. And extra viscous force around gaps dissipates the oscillation energy quickly.

Acknowledgments

The authors are grateful for the support of the National Basic Research Program (91441123) and The Test Technology Research Program (2015SY41B0005) in funding this research.

References

[1]. Harrje, D., and Reardon, F., "Liquid Propellant Rocket Combustion Instability," NASA SP-194, 1972.

[2]. Oefelein, J., and Yang, V., "Comprehensive Review of Liquid-Propellant Combustion Instabilities in F-1 Engines," [J] Journal of Propulsion and Power, Vol. 9, No. 5, 1993, pp. 657–677.

[3]. V Yang, W E Aderson, Liquid rocket engine combustion instability [M]. Reston: AIAA, 1995.

[4]. CH Sohn, SK Kim, YM Kim, Effects of various baffle designs on acoustic characteristics in combustion chamber of liquid rocket engine [J]. Journal of Mechanical Science and Technology, 2004, 18(1):145-152.

[5]. J. D. Anderson. Computational Fluid Dynamics: The Basics with Applications. [M]. TSING HUA UNIVESITY, 2010.

[6]. Cai Hong-hua, Nie Wan-sheng, Zheng Gang. Impact of the inner nozzle surface on plume characteristics of LOX/kerosene engine [J]. Missile and Space Vehicles, 2015(5): 35-38.

[7]. Piscaglia F, MOntorfano A, Ferrari G, et al. High resolution central schemes for multi-dimension nan-linear acoustic simulation of silencers in internal combustion engines [J]. Mathematical and Computer Modeling, 2011, 54, 1719-1725.

[8]. Magnussen B F, Hjertager B H. On mathematical models of turbulent combustion with special emphasis on soot formation and combustion[C]. 16th Symposium (Int) on Combustion, Cambridge, MA, 1976, (1): 719-729.

[9]. Wang, T S, Farmer, R C, Edelman R B. Turbulent combustion kinetics for complex hydrocarbon Fuels [C]. AIAA 26th Aerospace Sciences Meeting, Reno, USA, JAN 11-14, 1988.

[10]. VL Zimont. Gas Premixed Combustion at High Turbulence. Turbulent Flame Closure Combustion Model. [J] Experimental Thermal & Fluid Science, 2000, 21(1–3): 179-186.

[11]. Harvazinski, M., Anderson, W., Merkle, C. et al, "Combustion Instability Diagnostics Using the Rayleigh Index," 47thAIAA/ASME/SAE/ASEE Joint Propulsion Conference and Exhibit, San Diego, CA, July 2011, AIAA Paper 2011-5548.

[12]. Smith, R., Xia, G., Anderson, W., Merkle, C., et al "Extraction of Combustion Instability Mechanisms from Detailed Computational Simulations," 48th AIAA Aerospace Sciences Meeting Including the New Horizons Forum and Aerospace Exposition, AIAA-2010-1152, Orlando, Florida, Jan. 4-7, 2010.

[13]. DH Huang, DK Huzel. Modern Engineering for Design of Liquid-Propellant Rocket Engines. [M] American Institute of Aeronautics & Astronautics. 2015, 130-132

[14]. KJ Lee, JK Hong, S Seo, et al. Experimental Verification for Acoustic Damping Enhancement by Gaps in Injector-Formed Baffles [J]. Journal of Propulsion & Power, 2014, 25(2): 435-442.

[15]. IS Park, CH Sohn, JK Hong, Acoustic damping enhanced by gaps in baffled injectors in an acoustic chamber [J]. Journal of Sound & Vibration, 2011, 330(12): 2747-2757.

[16]. I Park, CH Sohn, "A Numerical Study on Acoustic Damping Mechanism of Baffled-Injectors in an Acoustic Chamber." 46th AIAA/ASME/SAE/ASEE Joint Propulsion Conference & Exhibit, Joint Propulsion Conferences

[17]. JK Hong, KJ Lee, HS Choi, et al. "An Experimental Study on Acoustic Damping Enhancement by the Gap of Baffled Injectors." 41st AIAA/ASME/SAE/ASEE Joint Propulsion Conference & Exhibit, Joint Propulsion Conferences